Pergamon

PII S1359-6454(96)00012-2

Acta mater. Vol. 44, No. 9, pp. 3667–3677, 1996

Published by Elsevier Science Ltd

1359-6454/96 $15.00 + 0.00

PLASTIC INSTABILITY IN AN OMEGA FORMING Ti–15% Mo ALLOY

S. BANERJEE and U. M. NAIK

Metallurgy Division, Bhabha Atomic Research Centre, Bombay 400 085, India

(Received 20 June 1995; in revised form 28 November 1995)

Abstract—The plastic flow behaviour of a β-titanium alloy (Ti–15% Mo) was investigated over a wide range of temperatures and strain rates covering those conditions where the ω-phase forms dynamically. Portevin–Le Chatelier (PLC) effect was observed in this alloy at temperatures between 575 and 775 K at a strain rate of $1.31 \times 10^{-4}\ s^{-1}$. The serrated flow behaviour of this alloy could be suppressed by rendering the matrix β-phase more stable against the β to ω transformation. PLC bands formed in this alloy, studied at different levels of magnification using light, scanning electron and transmission electron microscopy, showed a high density of deformation bands within the macroscopic PLC band. The following mechanism of serrated flow is proposed: the load drop is ascribed to the sudden flow associated with the formation of deformation bands within which ω-particles were destroyed while the subsequent load rise results from pinning of dislocations by ω-particles forming dynamically.

1. INTRODUCTION

Instabilities in plastic deformation under a monotonic loading can be classified [1–3] into the following two broad types.

(a) Instabilities related to local strain softening result from a sudden increase in the mobile dislocation density within localized deformation bands. Rapid multiplication of dislocations in whiskers, sudden release of dislocations from pinning centres and precipitate shearing processes are responsible for such a flow which is associated with a negative local strain hardening coefficient.

(b) Instabilities can arise from a negative strain rate sensitivity behaviour. Dynamic interactions between dislocations and diffusing solute atoms are generally responsible for this type of instability, which is known as the Portevin–Le Chatelier (PLC) effect [4] characterized by the occurrence of discontinuous or serrated yielding.

In recent literature there has been a discussion [3, 5] regarding the possibility of some microscopic mechanisms giving rise to both the aforementioned instabilities. The PLC effect in substitutional alloys has generally been attributed to a periodic locking and unlocking of dislocations by solute atoms [6–8]. Since this process involves long range diffusion of solute atoms, enhanced diffusivity due to plastic flow has been invoked for explaining the kinetics of the process [6]. Numerous experimental observations showing the presence of a critical strain, ϵ_c preceding the appearance of serrated yielding have provided support to the diffusivity enhancement model [7]. McCormick [9] has proposed that quasistatic ageing of dislocations occurs during the waiting time, t_w of dislocations between two successive obstacles. This concept was extended by Van den Beukel [8] incorporating a thermally activated strain rate equation where the activation enthalpy is assumed to depend on both the effective stress and the local solute concentration near the dislocation. Mulford and Kocks [10] have proposed an alternative approach in which the strain rate sensitivity is described in terms of two components—the friction stress σ_f and the dislocation flow stress σ_d. The latter component, which is negative from the beginning, dominates after the attainment of ϵ_c and makes the total strain rate sensitivity negative.

The occurrence of the PLC effects has been treated on the basis of collective movement of a group of dislocations by Schoeck [11] and of propagation of localized deformation bands by Schlipf [12]. Also there have been reports in which locking is effected not by individual solute atoms but by clusters of solute atoms [13, 14]. However, it has still not been established whether the precipitate shearing mechanism which is known to introduce local strain softening can lead to the PLC effect. Discontinuous yielding observed in aluminium–lithium binary alloys containing shearable precipitates [15, 16] are still not clear examples of precipitate shearing being directly responsible for the PLC effect.

Gysler *et al.* [17] have shown that the plastic deformation of a $\beta + \omega$ structure with a distribution of fine ω particles in Ti–15% Mo results in the creation of shear bands within which ω particles are destroyed. In spite of the low macroscopic ductility, substantial plastic flow on localized shear bands was revealed from the operation of the microvoid coalescence mechanism on the terraced shear bands

observed on the fracture surface of the Ti–15% Mo alloy in the ω aged condition [17]. Since the ω precipitation is known to be quite rapid in the temperature range of 575–775 K [18] and these precipitates can have strong elastic interactions with dislocations [17], the present experiments have been planned for exploring whether dynamic locking of dislocations in shear bands is possible in an ω forming system leading to serrated yielding in appropriate ranges of temperatures and strain rates.

2. EXPERIMENTAL

Alloy ingots of nominal compositions, Ti–15%, Mo and Ti–25% Mo were prepared by non-consumable arc melting and were hot rolled and subsequently cold rolled into thin strips of about 0.3 mm thickness. Chemical analyses of the samples studied are given in Table 1. Tensile test pieces of 12.5 mm gauge length were machined from this strip. All tensile test specimens and small samples for metallographic examinations were initially heat treated in the β quenched condition by soaking the samples sealed in He filled quartz capsules at 1073 K for 30 min followed by water quenching. Some of these β quenched samples were subsequently aged at two temperatures, 575 and 875 K for precipitating the ω phase and the α phase, respectively. These samples will henceforth be referred to as the ω-aged and the α-aged samples, respectively.

Tensile testing of these samples was carried out in the temperature range of 300–773 K in an Instron screw driven testing machine employing different cross head speeds ranging from 0.005 to 0.5 cm/min. The testing temperature was controlled within $\pm$ 2 K and zero suppression of the load sensed was used for recording the nature of the serrated behaviour. In order to study the nature of the PLC band and the sequence of their formation, some samples were polished for metallographic observations before testing. These samples were unloaded immediately after the appearance of a few load drops.

The characterization of the microstructure of the Ti–15% Mo alloy in different heat treatment conditions was carried out by transmission electron microscopy (TEM) of samples heat treated along with the tensile test specimens. Discs of 3 mm diameter were punched from the PLC band regions of tensile test samples for studying the microstructure of the deformed regions. TEM samples were prepared by dual jet electropolishing in an electrolyte containing perchloric acid, *n*-butanol and methanol maintained at around 240 K.

Table 1. Chemical compositions of alloys

Ti–Mo samples	Molybdenum wt%	Oxygen wt%	Nitrogen wt%
Ti–15 Mo (A)	15.2	0.164 $\pm$ 0.005	0.008
Ti–15 Mo (B)	15.5	0.15	0.05
Ti–25 Mo	24.6	0.14	0.05

3. RESULTS

3.1. Microstructures and room temperature deformation behaviour of Ti–15% Mo in different heat treated conditions

In the β quenched condition the alloy exhibits a structure [Fig. 1(a)] consisting of fine particles of ω phase distributed in equiaxed β grains. These ω particles having the size range 2–5 nm in diameter are known to have originated from an athermal displacive β–ω transformation during the quenching process [19]. Corresponding diffraction patterns show ω and β reflections in addition to the intensity streaks, characteristic of a structure containing athermal ω in the β matrix. On ageing, precipitation of either the metastable ω phase or the equilibrium α phase occurs depending on the ageing conditions. The structure produced on ageing at 575 K for 30 min shows a distribution of aged ω particles in the β matrix [Fig. 1(b)]. Omega particles produced during quenching and ageing will henceforth be referred to as athermal-ω and aged-ω, respectively. Precipitation of the α phase occurs in samples aged at 875 K for 0.25 h as illustrated in Fig. 1(c).

A comparison of the stress–strain plots at 300 K of Ti–15% Mo in these three different microstructural states reveals that (i) the β + athermal–ω structure is associated with a low yield strength ($\simeq$650 MPa) and an extensive elongation ($\simeq$40%); (ii) the β + aged–ω structure exhibits a significant increase in yield strength ($\simeq$1200 MPa) and a drastic reduction in elongation ($<$5%); while (iii) in the α-aged structure marginal improvements both in elongation ($\simeq$8%) and strength ($\simeq$1300 MPa) are observed.

3.2. Flow behaviour of the β-quenched alloy in the temperature range, 300 K $<$ T $<$ 775 K

The stress–strain plots for the β quenched Ti–15% Mo samples tested at different temperatures at a nominal strain rate of $1.31 \times 10^{-4}\,s^{-1}$ are shown in Fig. 2. The most striking feature of these stress–strain (σ versus ϵ) plots is that in a certain temperature range (575–725 K for the strain rate $1.31 \times 10^{-4}\,s^{-1}$) pronounced periodic serrations appear in the flow curves. The ranges of strains over which the serrated flow behaviour have been observed are indicated on the flow curves schematically by small vertical segments representing extents of stress drops. The magnified load–elongation plot shown in the inset reveals that the load drop occurs from load levels which can be joined by a hypothetical upper envelope. It is also seen that flow curves showing serrations are associated with lower work hardening rates. Based on the classification scheme proposed by Brindley and Worthington [7] the observed serrations can be designated as C-type.

The 0.2% yield stress and the total elongation has been plotted against the testing temperature in Figs 3(a) and (b). It may be noted that the descending part

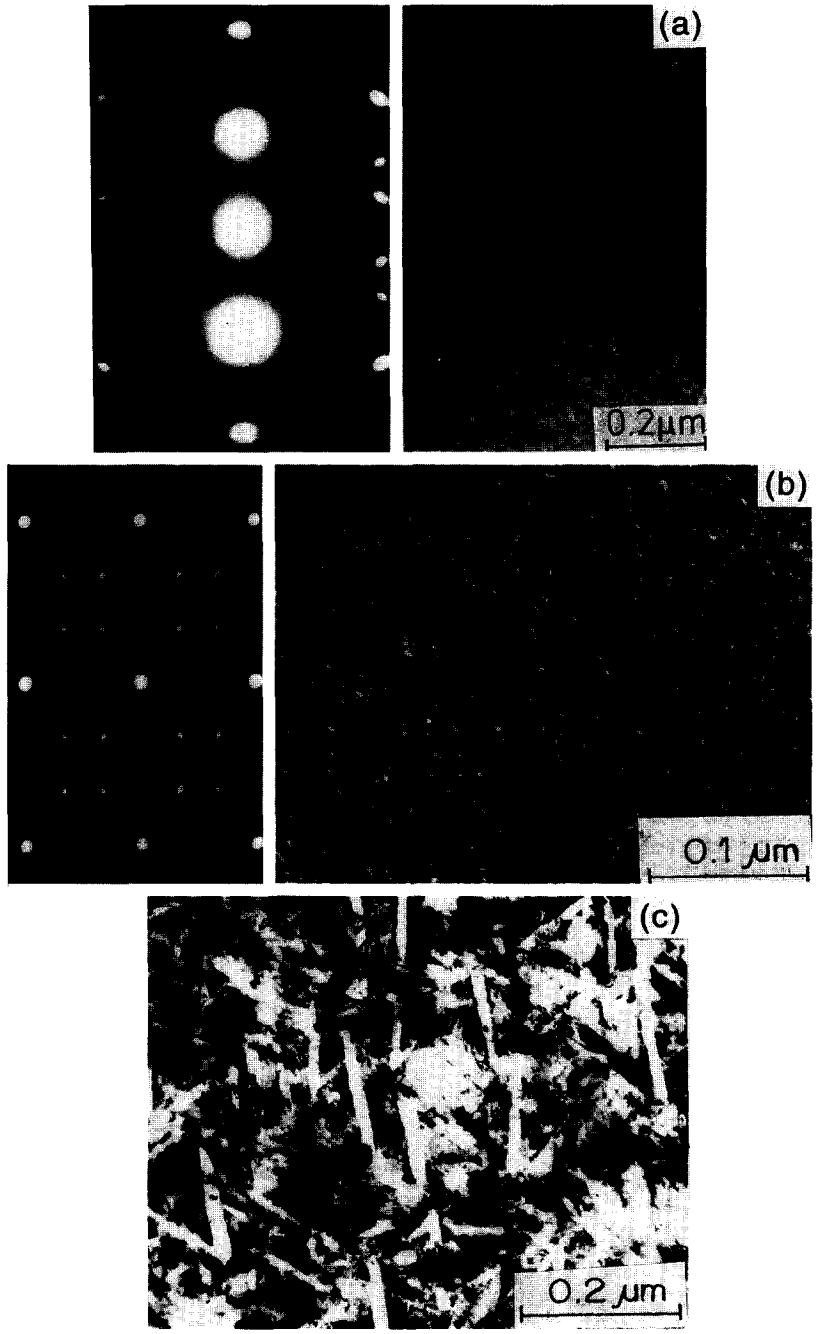

Fig. 1. Microstructure of Ti–15% Mo in different heat treatment conditions. (a) The β-quenched state shows a distribution of fine athermal ω-particles (in bright contrast under dark field imaging with an ω-reflection) and a diffuse intensity distribution along with β-reflections characteristic of the β + athermal ω structure; (b) ω-aged structure (575 K for 1 h) shows ω-precipitates in the β matrix and sharp ω reflections; (c) α-aged structure shows α-plates distribution in the β matrix in the sample aged at 875 K for 15 min.

of the hump in the yield stress versus testing temperature plot corresponds to the temperature range of serrated flow.

The critical plastic strain, ϵ_c that is required for the initiation of the serrated flow has been measured for different strain rates and testing temperatures and the data are presented in an ϵ_c versus $1/T$ plot and in an ϵ_c versus $\ln(\dot{\epsilon})$ plot [Figs 3(c) and (d)]. The observed dependence of ϵ_c on T and $\dot{\epsilon}$ exhibits a "normal" behaviour which is in contrast to those encountered in C-type serrated flow. This point is discussed in a later section.

3.3. Temperature–strain rate regime for serrated flow

Tensile testing of β-quenched samples has been carried out in wide ranges of temperatures and strain rates and, corresponding to each combination of test variables, a circle is marked in a plot of $\ln \dot{\epsilon}$ versus $1/T$ (Fig. 4). Circles are drawn filled or open depending on whether serrated flow occurs in the given condition of temperature and strain rate. It is then possible to mark three distinct regions, of which only the central hatched region defines the serrated flow regime. It needs to be emphasized that in the present case serrated flow is seen to persist from the ϵ_c value to the point of fracture.

3.4. Formation of PLC bands

Some prepolished samples were unloaded after the appearance of a few distinct load drops. On the examination of the gauge length of these samples under a light microscope, it was found that a few PLC bands had formed [Fig. 5(a)]. A one to one correspondence between the number of serrations and the number of PLC bands could be obtained only in the initial stage. Within the macroscopic PLC band beta grains get revealed due to the offsets created at grain boundaries [Fig. 5(a)]. Each of these grains show a distribution of finer deformation bands which show the following characteristics:

(i) these bands which are often found to be in parallel groups do not cross the grain boundaries;
(ii) they are not perfectly straight;
(iii) their population density is found to be a maximum in the centre of a PLC band [Fig. 5(b)] and to decrease as the PLC band boundary [Fig. 5(c)] is approached;
(iv) scanning electron microscopy revealed the presence of steps [Fig. 5(d)] along directions in which these bands intersect the polished sample surface. These steps can be polished off and the polished and etched surface of the deformed samples do not show these bands, indicating that they correspond to neither deformation twins nor stress induced martensite plates.

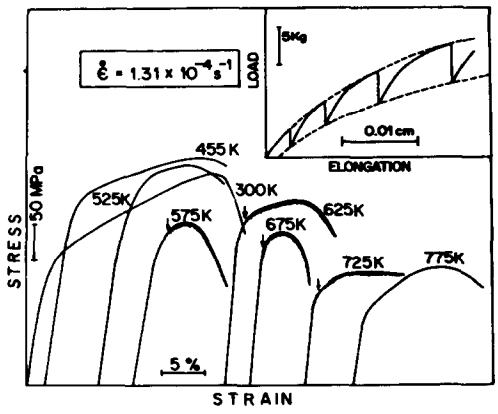

Fig. 2. Stress–strain plots for the β-quenched Ti–15% Mo samples tested at different temperatures (as indicated alongside the flow curves) and at a strain rate of $1.31 \times 10^{-4} s^{-1}$. Serrated flow indicated by short vertical lines on the flow curves is observed in the temperature range 575–725 K. Arrows are marked at the onset of serrated flow. The inset shows a magnified portion of a load–elongation plot.

3.5. Strain rate sensitivity

It has been suggested that the jerky flow occurs only when conditions conducive to unstable deformation are present. Following the method proposed by Mulford and Kocks [10], strain rate sensitivity was measured at different testing temperatures and for different levels of stress. A plot of the strain rate sensitivity, $(\Delta\sigma/\Delta \ln \dot{\epsilon})$ versus stress, σ (Fig. 6) shows that the former changes from a positive to a negative value with increase in σ at testing temperatures of 550 and 575 K. The cross-over point is seen to correspond to the critical strain value. At higher temperatures where serrated behaviour is observed right from the onset of plastic flow, strain rate sensitivity is seen to be negative in the entire plastic flow regime.

3.6. Deformation behaviour of aged samples at elevated temperatures

Omega-aged samples which show very little tensile elongation at room temperature exhibit much higher elongation when tensile testing is carried out in the temperature range of 550–725 K. Serrated flow behaviour also persists in ω-aged samples (Fig. 7) though the magnitude of stress drops is seen to decrease with increasing ageing time [flow curves (a)–(c) in Fig. 7]. Serrated flow behaviour is seen to be completely suppressed in α-aged samples [flow curve (d) in Fig. 7].

3.7. Static ageing experiments

Static ageing experiments were carried out by allowing the ageing process to occur on load (i.e. by arresting the cross head motion during the serrated flow process) and recording the load as a function of time. The test is essentially similar to the stress relaxation test as described in Ref. [20]. Results of such experiments as illustrated in Fig. 8(a) show that the stress initially relaxes with time and subsequently rises. As the stress value approaches the upper envelope of the flow curve, a sudden drop in stress is noticed. This is followed by an increase in stress till a second load drop occurs. Such repeated load drops continue to occur to produce a serrated appearance of the stress versus time plot. The relaxation plots corresponding to two strain values, (i) prior to and (ii) subsequent to the appearance of serrated flow, are also compared in Fig. 8. In both cases, the general trend of initial stress relaxation followed by a rise in stress is noticed. The stress in the former case [Fig. 8(b)], however, could not rise to a value to cause abrupt load drops as encountered in the latter case [Fig. 8(a)].

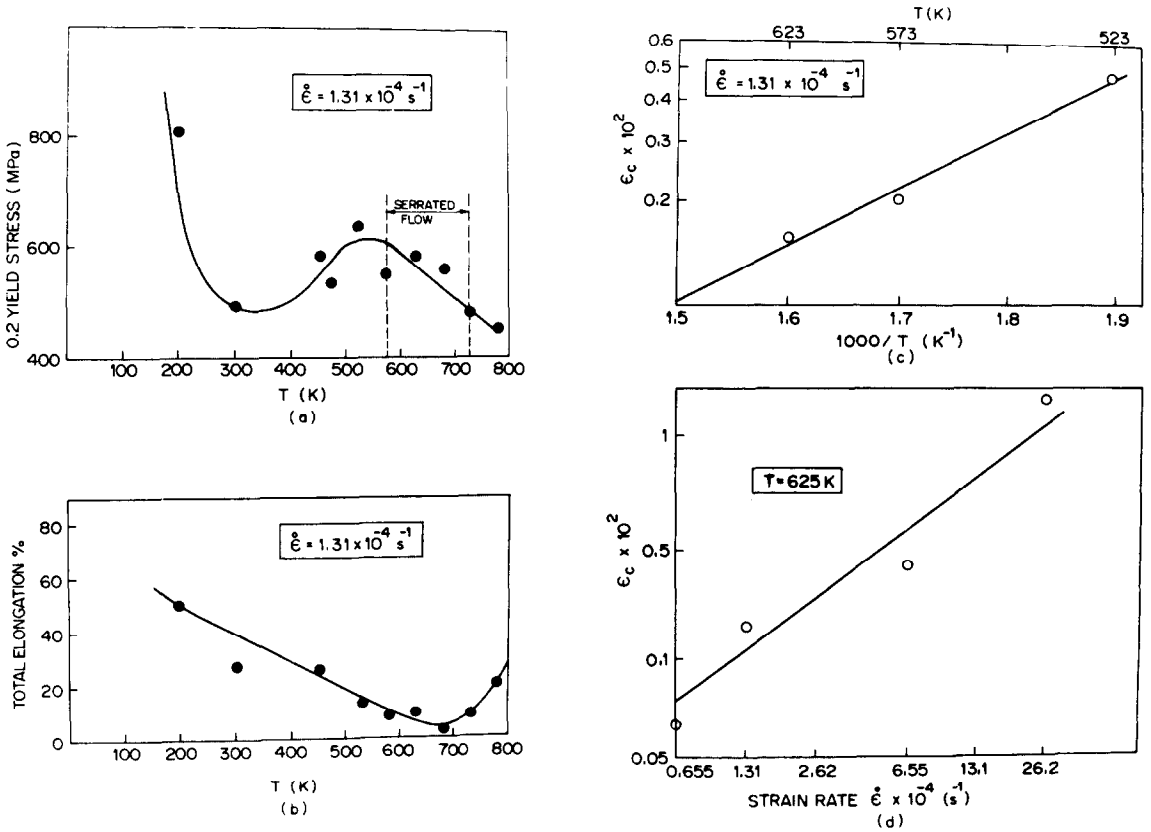

Fig. 3. (a) 0.2% yield stress plotted against testing temperature shows a hump in the temperature range 450–675 K which nearly coincides with the temperature range of serrated flow, 575–725 K. (b) A minimum in the total elongation is observed at 675 K. Part (c) shows critical strain (ϵ_c) for the onset of serrated flow as a function of reciprocal temperature ($1/T$) and (d) shows ϵ_c as a function of strain rate ($\dot{\epsilon}$).

3.8. *Deformation behaviour of Ti–25% Mo*

The β quenched Ti–25% Mo alloy exhibits a full β structure which does not contain any athermal ω phase. The β phase in this alloy does not precipitate out the ω phase during ageing in the temperature range 575–775 K. Deformation behaviour of this alloy was studied with a view to examining whether the serrated yielding phenomenon is encountered in a fully β stabilized alloy. Tensile testing of Ti–25% Mo samples in the temperature range of 575–775 K at strain rates ranging from 6.6×10^{-6} to 6.6×10^{-4} s^{-1} showed that serrated yielding did not occur in any combination of temperature and strain rate.

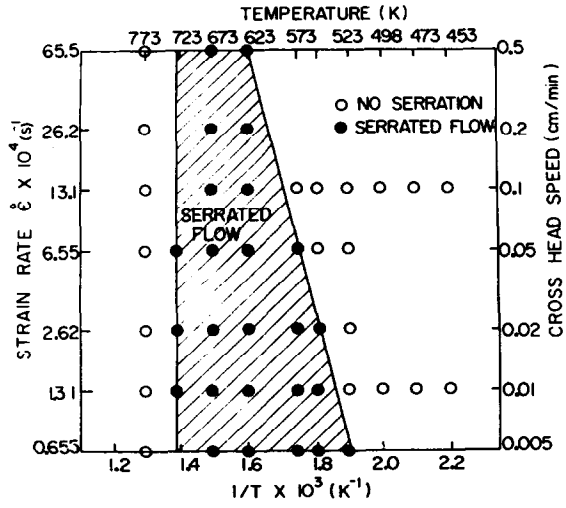

Fig. 4. Strain rate–temperature regime in which serrated flow is observed in Ti–15% Mo.

3.9. *Microstructures of samples deformed at 300 and 573 K*

About 2% plastic strain at 300 K results in the formation of a planar dislocation arrangement in the β quenched Ti–15% Mo alloy. Such planar arrangements of dislocations are consistent with the flow mechanism in which leading dislocations clear away obstacles present in the slip path facilitating easy glide of trailing dislocations along the obstacle free channels [17].

Samples tested in the temperature range, 575–725 K, showed aged ω particles which were as large as 5–20 nm in diameter. The total time required for equilibration of tensile test samples with the furnace

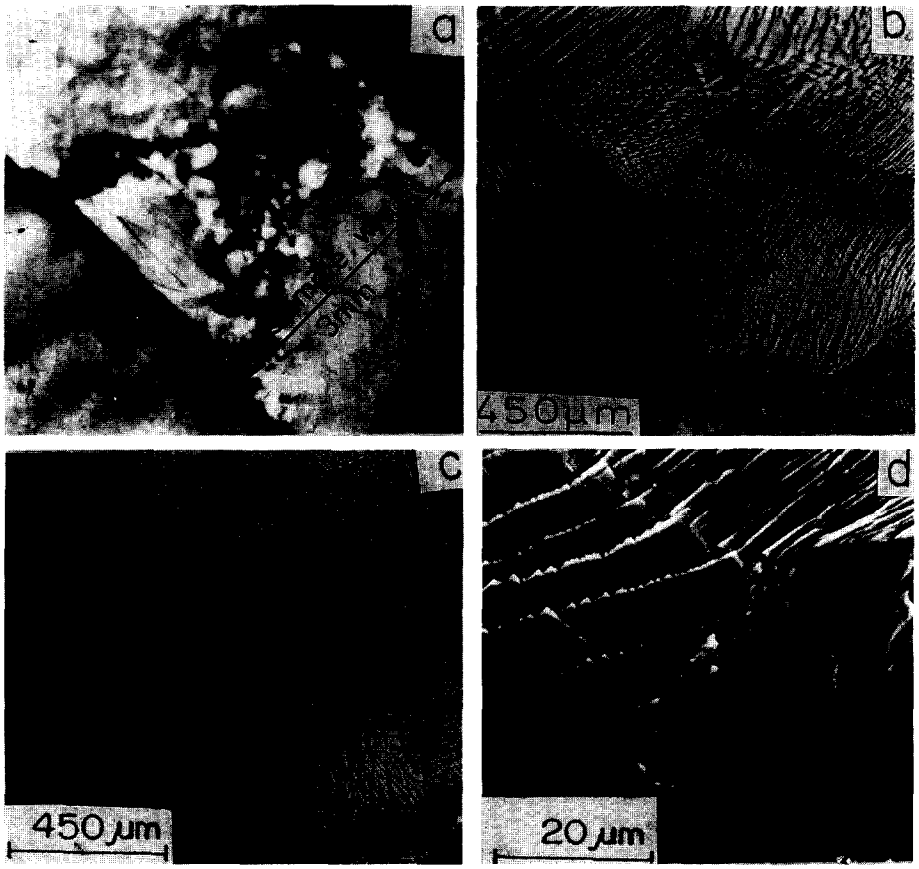

Fig. 5. (a) Macroscopic PLC bands in a sample unloaded after the appearance of two load drops in the stress–strain plot. The β-grain structure is revealed within the PLC band. (b) Finer deformation bands seen within the grains inside a PLC band. (c) Smaller density of deformation bands at the boundary of the PLC band. (d) Scanning electron micrograph showing steps formed on the polished surface by deformation bands.

temperature and for testing ($\simeq$30 min) was sufficient for the growth of aged ω particles to this extent [Fig. 1(b)]. Due to the limited tensile ductility of such samples at 300 K, they could not be subjected to a high plastic strain by tensile deformation. Hence these samples were given cold rolling to introduce a heavy deformation (about 30% reduction in thickness). Thin edges of the electropolished specimens taken from such deformed material were imaged in the dark field using a prominent ω reflection. Microscopic deformation bands devoid of ω particles were revealed under this imaging condition [Figs 9(a) and (b)]. An intense dislocation activity resulting from the localized flow within the bands is noticed in images taken with the matrix β reflections. On tilting the sample to make the deformation band nearly parallel to the electron beam, the typical thickness of a microscopic deformation band can be viewed. The manner in which individual ω particles are destroyed along such a band is clearly seen in Fig. 9(b). Some deformed samples were subsequently aged for short times up to 15 min. Imaging of deformation bands in these samples showed restoration of ω particles [Fig. 9(c)]. The observation that only ω particles within the band are in contrast suggests that the orientation of the β-region within the deformation band has changed to a certain extent with respect to that of the matrix β grain.

The localized plastic flow in the ω-aged samples deformed at room temperature is reflected in the morphology of fractured surfaces which show steps created by deformation bands. Tensile ductility is considerably restored when the testing temperature is raised to 625 K. Plastic flow does not remain confined within localized deformation bands and the morphology of fracture surfaces show typical dimple structure characteristic of the microvoid coalescence mechanism. A comparison of the fracture morphologies has been made in an earlier paper [21].

4. DISCUSSIONS

4.1. The origin of serrated flow

Possible mechanisms of discontinuous yielding are first examined in order to find out whether the observations listed earlier can be attributed to any of these mechanisms.

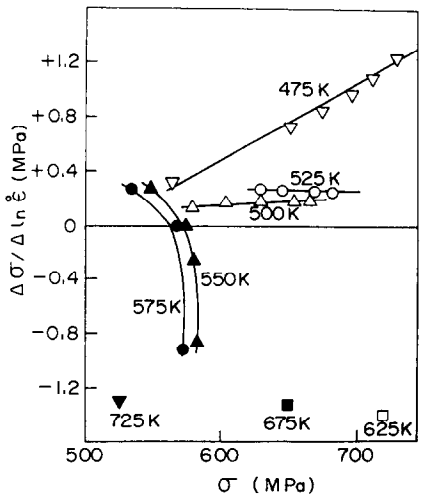

Fig. 6. Strain rate sensitivity $\Delta\sigma/\Delta\ln\dot{\epsilon}$ vs stress plot shows a decreasing tendency of the former at 550 and 575 K, reaching a negative value as serrated flow begins.

4.1.1. Dislocation–solute atom interactions. Serrated yielding can result from a process involving repeated locking and unlocking of dislocations by interstitial and substitutional solutes, the upper yield stress representing the stress required for freeing dislocations from the solute atmosphere. The process is operative under conditions where the rate of solute migration is sufficiently high to enable pinning of dislocations while they are temporarily waiting at obstacles for required thermal activation. The difference between the mechanism of serrated yielding due to substitutional and interstitial solutes arises due to the differences in their diffusivities. However, neither the substitutional nor the interstitial solute atom interactions with dislocations can explain the following experimental observations:

(i) serrated flow behaviour can be completely or partially suppressed in Ti–15% Mo when the alloy is either α-aged or ω-aged for long durations;

(ii) the Ti–25% Mo alloy did not exhibit serrated flow in the entire strain rate–temperature regime studied in the present work, though interstitial contents in this alloy were about the same as that in Ti–15% Mo;

(iii) the upper temperature limit of the strain rate–temperature regime for serrated flow in Ti–15% Mo is independent of the strain rate. This is unusual for a solute pinning mechanism.

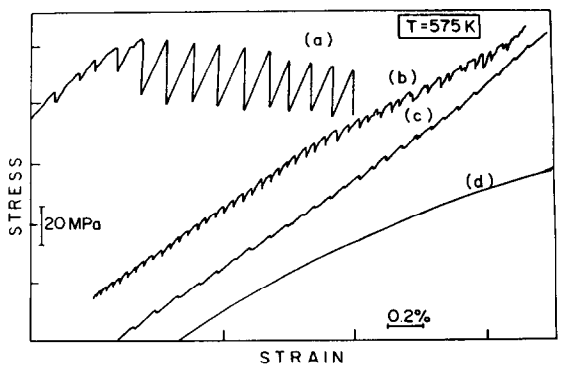

Fig. 7. The influence of ageing treatment on the amplitude of serration is seen from the parts of the flow curves at 575 K of Ti–15% Mo heat treated at different ageing conditions. (a) 575 K for 1 h; (b) 675 K for 1 h; (c) 675 K for 168 h; and (d) 875 K for 1 h.

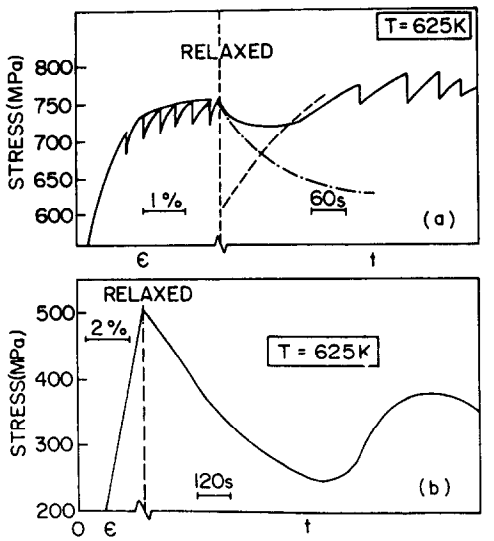

Fig. 8. The influence of the on-load static ageing treatment on the stress–strain diagram. (a) In the case where ageing treatment/relaxation is commenced after a few serrations in the flow curves have appeared. (b) In the case when the sample is relaxed at a point where plastic flow has not commenced.

4.1.2. Load drops associated with sudden plastic flow caused by athermal processes like deformation twinning or stress assisted martensitic transformation. In general, the formation of deformation twins and stress assisted martensite plates requires a higher stress for their nucleation than for their growth. The burst of plastic flow which follows the nucleation event results in load drops in the flow curve. However, these mechanisms cannot explain the following observations made in the present study.

(i) The serrated yielding process in Ti–15% Mo is thermally activated, whereas deformation twinning or martensite formation are athermal. In fact the latter two processes are expected to be favoured at lower temperatures.

(ii) No deformation twin or martensite plate could be detected within PLC bands.

4.1.3. Serrated yielding due to ω precipitation. The observations which suggest the connection between serrated yielding and dynamic precipitation of ω phase are as follows.

(i) The temperature range for rapid ω precipi-

tation and that for the occurrence of serrated yielding, particularly the upper cut off temperatures ($\sim$775 K) for both match very closely.

(ii) The observation that the intensity of serrations can be either reduced by prior ω-ageing or completely suppressed by a prior α-ageing treatment points to the fact that an increased stability of the β-matrix (as a result of molybdenum enrichment consequent to ω or α precipitation) can suppress serrated yielding. This point is also demonstrated by the absence of serrated flow in Ti–25% Mo.

(iii) Deformation bands within which ω particles are destroyed could be seen in ω-aged samples deformed at room temperature. Restoration of ω precipitates within deformation bands on subsequent ageing is also observed.

(iv) Evidence for the dynamic ω precipitation during the on-load ageing experiment has been obtained.

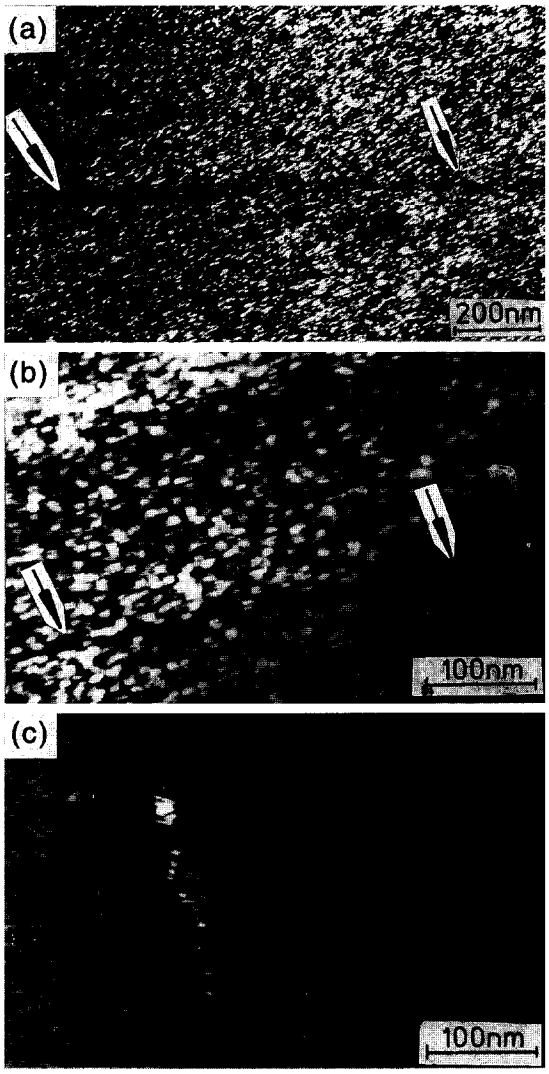

Fig. 9. TEM microstructures of microscopic deformation bands. (a) A reduced density of ω-particles is seen within the deformation band, imaged under dark field using an ω-reflection. (b) Edge-on view of a deformation band showing the true thickness of the band. (c) Restoration of omega particles within a deformation band after reageing.

Based on these observations, the following mechanism of the serrated flow in Ti–15% Mo is proposed. The suitability of this mechanism in explaining the experimental findings is discussed subsequently.

4.2. *The proposed model*

Most of the treatments on the serrated flow behaviour of alloys are based on interactions of individual dislocations with diffusing solutes. In the present case, however, neither dislocation pinning by solute atoms nor mobilization of individual dislocations are responsible for serrated flow. It is envisaged that the dislocation pinning process is caused by ω particles which form dynamically during elevated temperature testing and sudden burst of plastic flow occurs when deformation bands are created by shearing of ω particles within these bands. As shown by structural observations, the macroscopic plastic instability manifests itself at different length scales. In the finest scale, a single ω free channel is created by the passage of an avalanche of dislocations, a typical soft channel being a few nanometers thick. A group of such channels constitute a deformation band (typically several micrometers thick) which can be resolved under a light microscope. These deformation bands remain confined within the β-grains, but the strain compatibility between neighbouring grains is responsible for triggering plastic flow in the adjacent grains through the same microscopic mechanism. As a result of this deformation event, a macroscopic PLC band (in millimeter scale) is formed. A single load drop which is associated with the creation of a PLC band in the initial stages of plastic flow corresponds to a sudden release of a large number of dislocations and their simultaneous motion. This is feasible as the creation of soft channels free of ω particles provides easy passage of dislocations which follow the shear front of deformation bands. The model is therefore based on a description involving the movement of an ensemble of dislocations in a material containing second phase particles which are sheared during the deformation process and the dynamic restoration of ω particles within these soft channels to cause further pinning.

Gysler *et al.* [16] have shown that the stress required for shearing of ω particles in the Ti–11% Mo alloy containing a distribution of ω precipitates (4–10 nm in diameter and the volume fraction of the ω phase being within 0.05 and 0.35) is less than that required for dislocations for bypassing [22]. They have also shown that ω free deformation bands are produced in such a structure after deformation at

300 K. The present work has demonstrated that restoration of these particles is also possible when deformation is carried out in the temperature–strain regime of serrated yielding.

The macroscopic strain rate, $\dot{\epsilon}$ is related with the density ρ_m, the average velocity, v and the Burgers vector, b of moving dislocations by the following equation

$$\dot{\epsilon} = \rho_m b v. \tag{1}$$

The average velocity of moving dislocations in a material containing a distribution of dislocation pinning obstacles can be expressed as

$$v = l/(t_w + t_f) \sim l/t_w \tag{2}$$

where l is the mean free spacing between obstacles, t_w is the average waiting time at obstacles and t_f ($\ll t_w$), the time of flight of dislocations from one obstacle to the next.

The samples tested in the serrated yielding regime were exposed to the test temperature for about 20 min prior to the commencement of straining and this had resulted in the formation of fine aged ω precipitates. The first load drop corresponds to the formation of a PLC band within which a number of microscopic deformation bands (channels of ω-free region) are triggered. At temperatures below the serrated flow regime localized flow within these deformation bands continues leading to fracture at a very low elongation. Though considerable plastic flow as revealed in the dimple structure on facets of the fracture surface occurs within the deformation bands, the macroscopic elongation remains very limited due to the localized nature of flow.

In the serrated flow regime, plastic flow within deformation bands cannot continue up to the point of microvoid nucleation as the dynamic restoration of ω particles gradually pin the moving dislocations, their density decreasing with time causing corresponding increase in stress. The Portevin–Le Chatelier effect in terms of the density of mobile dislocations has been discussed by Schoeck [11]. It is shown that an instability of plastic flow (accompanied by negative strain rate sensitivity) exists in the neighbourhood of a critical value, ρ_p, of the mobile dislocation density where

$$t_w/t_p = \rho_m/\rho_p, \tag{3}$$

t_w being the average value of waiting time and t_p the average ageing time for pinning a dislocation. The same argument can be invoked in describing the plastic flow within the localized deformation bands in the present case. When the kinetics of the ω formation are favourable, the time (t_p) required to pin dislocations by restoration of ω particles along the deformation bands becomes less than the waiting time t_w. Under this condition, as the plastic flow continues within a given

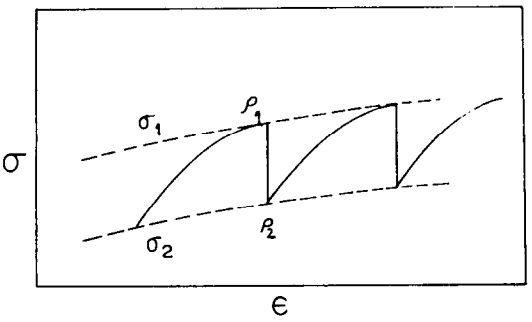

Fig. 10. Schematic stress (σ) versus strain (ϵ) diagram within a localized deformation band. σ_1 represents the threshold stress required for triggering a deformation band.

deformation band subsequent to a load drop event, more and more dislocations become pinned and the stress required to sustain the strain rate gradually rises. The flow within a deformation band at a constant $\dot{\epsilon}$ can be schematically represented in a "local" stress–strain plot (Fig. 10) in which the flow stress, σ_2 corresponds to the high mobile dislocation density (ρ_2) within an ω-free channel, immediately after the creation of deformation band and the threshold stress, σ_1 at which ω-particles are sheared are indicated by dashed lines. The observed load drop then corresponds to σ_1–σ_2 and flow stress rises from σ_2 to σ_1 as ρ_m decreases from a higher (ρ_2) to a lower level (ρ_1) with increasing degree of pinning. The attainment of σ_1 triggers creation of fresh deformation bands or reactivates flow on the bands which have previously experienced a similar burst of dislocation mobilization. Successive operation of these processes leads to the serrated flow in which the maximum and minimum stress envelopes are given by σ_1 and σ_2 respectively.

As mentioned before, deformation bands observed in TEM microstructures are not just slip bands on single atomic layers, but are associated with a certain thickness. The entire volume associated with each deformation band can be viewed as a region where the displacement ordering related to ω particles is destroyed by the passage of a large number of dislocations. The tendency of restoration of ω particles in the deformation band arises from both the chemical driving force for ω precipitation and the elastic interaction between the strain fields associated with dislocations and favourably oriented ω particles. The displacement ordering process necessary for the production of the ω structure does not require any thermal activation at temperatures below the omega start temperature, ω_s which for Ti–15% Mo lies between 625 and 725 K. The observed thermal activation for dynamic restoration of ω particles can, therefore, be attributed to the solute segregation which is required prior to the displacement ordering. The formation of solute lean regions causes local increase in the ω_s temperature and thereby promotes the displacement ordering process.

4.3. Rationalization of experimental observations

Some important experimental observations are discussed in this section in terms of the proposed model.

4.3.1. Temperature dependence of flow stress. The observed hump in the flow stress versus temperature plot [Fig. 3(a)] corresponds to the temperature range 450–675 K in which precipitation hardening due to ω particles is most effective when the ageing time is nearly 30 min (duration of thermal equilibration and testing). For the serrated flow phenomenon the ageing time is essentially that between two successive serrations (in the range of 0.5–20 s). This explains why the serrated flow phenomenon occurs at a slightly higher temperature range 525–725 K which compensates for the shorter duration of ageing. At a given strain rate increasing the temperature from 525 to 675 K causes more effective dislocation pinning by ω particles. Beyond 675 K the ω-ageing process slows down due to a gradual shift from the ω to the α precipitation causing a reduction in the amplitude of serrations. Above 725 K precipitation of ω particles does not occur at all and therefore serrated yielding disappears.

4.3.2. Negative strain rate sensitivity. During serrated flow, as the strain rate is suddenly increased, the average velocity of moving dislocations increases by the same factor resulting in a sudden drop in the waiting time, t_w and a corresponding reduction in the size of ω particles which pin dislocations. The threshold stress required for cutting through a distribution of finer ω particles with a given spacing between the particles is smaller. This explains why an increase in the strain rate causes a lowering of the upper yield stress.

4.3.3. Critical plastic strain. The initiation of the serrated flow requires plastic strain to reach a certain critical value, ϵ_c. Brechet and Estrin [5] have recently examined the strain rate and the temperature dependences of ϵ_c for systems in which dislocations are pinned by precipitates. They have proposed a map showing different ranges of strain rate and temperature where the normal behaviour (ϵ_c increasing with $\dot{\epsilon}$ and decreasing with T) and the "inverse" behaviour are expected. The data from the present experiments are not sufficiently large to test the theory. However, the general trend in the present case is consistent with the normal behaviour which is expected in a system undergoing a homogeneous precipitation process. As the stability of the ω phase and the kinetics of its formation are both strongly related to the vacancy concentration [23, 24] the generation of vacancies by plastic deformation may also have a strong influence on the temperature and strain rate dependences of ϵ_c. Also from this consideration normal behaviour is expected. From the macroscopic deformation behaviour it has been established experimentally that serrated flow appears only when the strain rate sensitivity changes its sign from a positive to a negative value. This is essentially the condition for unstable plastic flow [10].

4.3.4. Activation energy. The activation energy of the ageing process was evaluated from the plot of $\ln(\dot{\epsilon}_0)$ against $1/T$ where $\dot{\epsilon}_0$ is the maximum strain rate at T at which serrated flow was observed. The experimental value of 30 kcal/mol is quite close to that reported (36 kcal/mol) for diffusion of molybdenum atoms in β-titanium alloys [25]. Since segregation of molybdenum atoms acts as a precursor to displacement ordering for the restoration of ω particles, the thermal activation required for the restoration process is essentially the same as that for molybdenum diffusion in the β matrix.

4.3.5. Static ageing under load. The observation of load rise with time followed by repeated load drops as observed during static ageing under load (see Section 3.7) can be interpreted as follows: during the serrated flow, as the cross head motion is arrested after a few serrations have appeared in the flow curve, the total strain rate, $\dot{\epsilon}_{tot}$ can be expressed as

$$\dot{\epsilon}_{tot} = \mathrm{d}/\mathrm{d}t\{\sigma/E + \epsilon_p + cf + M\sigma\} = 0 \qquad (4)$$

where the modulus, E, of the specimen is given by $(E_0 + f\Delta E)$, E_0 being the modulus at the start of the relaxation, ΔE being the difference between the moduli of the β and the ω phases and f is the volume fraction of the ω phase formed during time t; ϵ_p is the plastic strain of the specimen due to relaxation. The contraction of the specimen due to the dynamic ω formation is given by cf where c is a constant related to the 14% volume contraction associated with the β–ω transformation [23]. The last term in equation (4), $M\sigma$ is the strain contribution due to the elastic deformation of the testing machine, M being related to the stiffness of the machine.

The volume fraction, f of the ω phase after time t can be written as

$$f = f_\infty(1 - \mathrm{e}^{-t/\tau}) \qquad (5)$$

where τ is the time constant of the ω precipitation process and f_∞ is the equilibrium volume fraction of the ω phase. The relation between the plastic strain rate $\dot{\epsilon}_p$ and σ can be written as

$$\sigma = \sigma_1 + K \log \dot{\epsilon}_p/\dot{\epsilon}_0 \qquad (6)$$

where K is inversely proportional to the activation volume of the process. Substitution of some reasonable values as indicated in Table 2 yields a σ versus t plot (Fig. 11) showing an initial stress relaxation, followed by a rise in stress and then repeated stress drops as encountered experimentally (Fig. 8). The oversimplified treatment presented here qualitatively explains the relaxation behaviour due to the usual plastic flow and the competing rise in stress resulting from the contraction due to dynamic ω precipitation. When the latter part dominates the stress rises during the on-load static ageing process finally reaching the σ_1 value at which deformation

Table 2. Input parameters used for simulating the stress versus time plot during on-load ageing (Fig. 11)

Elastic modulus, E_0	50000 MPa
Modulus difference, ΔE	20000 MPa
Machine stiffness	50000 N/mm
Equilibrium ω volume fraction f_ω	10%
Time constant for ω formation, t_0	50 s [Fig. 11(a)] 100 s [Fig. 11(b)]
Threshold stress for formation of *deformation bands, σ_1	490 MPa

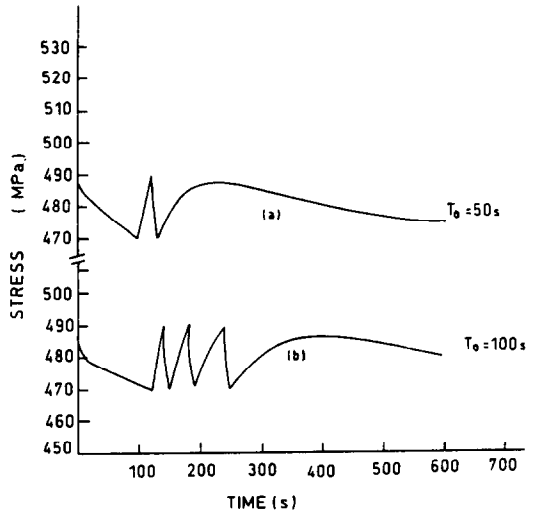

Fig. 11. Computed stress versus time plot for static ageing under load experiment. The parameters used for computation are given in Table 2.

bands are nucleated. The repeated occurrence of load drops in the stress–time plot can therefore be explained in terms of a combination of a stress relaxation and an ω-ageing process.

5. CONCLUSIONS

(1) The present experimental study demonstrates that a serrated plastic flow occurs in the Ti–15% Mo alloy under temperature and strain rate conditions favourable for dynamic formation of ω particles.

(2) The strain rate–temperature regime where the PLC effect is observed has been identified. While the low temperature limit of the serrated flow corresponds to the activation energy of diffusion of molybdenum, the upper cut off temperature matches with that for dissolution of ω particles.

(3) Experimental observations can be rationalized in terms of a mechanism involving creation of soft channels by shearing of ω particles and their dynamic restoration during mechanical testing.

(4) Plastic instability in this system has been found to occur at different length scales ranging from a few nanometers thick ω free channels to a few millimeters thick PLC bands.

Acknowledgements—The authors are grateful to Dr R. Krishnan, Mr V. V. Raman and Dr J. K. Chakravartty for many useful discussions during the course of the work. One of the authors (S.B.) is indebted to Professor L. Kubin for a detailed discussion on the experimental results. The support and encouragement received from Dr C. K. Gupta, Director, Materials Group, are gratefully acknowledged.

REFERENCES

1. Y. Estrin, in *Non Linear Phenomena in Materials Science* (edited by L. P. Kubin and G. Martin), p. 417. Trans. Tech. Publications, Aedermannsdort, Switzerland (1987).
2. Y. Brechet and F. Louchet, in *Non Linear Phenomena in Materials Science* (edited by L. P. Kubin and G. Martin). Trans. Tech. Publications, Aedermannsdort, Switzerland (1987).
3. Y. Brechet and Y. Estrin, *Scripta metall. mater.* **31,** 185 (1994).
4. A. Portevin and F. Le Chatelier, *C.r. Acad. Sci.* **176,** 507 (1923).
5. Y. Brechet and Y. Estrin, *Scripta metall. mater.* **31,** 185 (1995).
6. A. H. Cottrell, *Phil. Mag.* **44,** 829 (1953).
7. B. J. Brindley and P. J. Worthington, *Metall. Rev.* **4,** 101 (1970).
8. A. Van den Beukel, *Physica status solidi* (a) **30,** 197 (1975).
9. P. G. McCormick, *Acta metall.* **20,** 351 (1972).
10. R. A. Mulford and V. F. Kocks, *Acta metall.* **27,** 1125 (1979).
11. G. Schoeck, *Acta metall.* **32,** 1229 (1984).
12. J. Schlipf, *Acta metall. mater.* **40,** 2075 (1992).
13. R. Onodera, H. Era, T. Ishibashi and M. Shimizu, *Acta metall.* **31,** 1589 (1983).
14. R. Onodera, T. Ishibashi, H. Era and M. Shimizu, *Acta metall.* **32,** 817 (1984).
15. J. M. Gentzbittel and R. Fougeres, *Scripta metall. mater.* **21,** 1411 (1987).
16. L. P. Kubin, A. Stryczynski and Y. Estrin, *Scripta metall. mater.* **26,** 1423 (1992).
17. A. Gysler, G. Lutjering and V. Gerold, *Acta metall.* **22,** 901 (1974).
18. T. Yukawa, S. Ohtani, T. Nishimura and T. Sakai, in *Science Technology and Applications of Titanium* (edited by R. I. Jaffee and N. E. Promisel), p. 619. Pergamon Press. Oxford (1970).
19. S. L. Sass, *Acta metall.* **17,** 813 (1969).
20. I. Gupta and J. C. M. Li, *Mater. Sci. Engng* **6,** 20 (1970).
21. S. Banerjee, U. Naik and J. K. Chakravartty, *Key Engng Mater.* **103,** 267 (1995).
22. M. F. Ashby, in *Oxide Dispersion Strengthening* (edited by G. S. Ansell, T. D. Cooper and F. V. Lenel). Gordon and Breach, Oxford (1968).
23. S. K. Sikka, Y. K. Vora and R. Chidambaram, *Prog. Mater. Sci.* **27,** 245 (1982).
24. G. K. Dey, D. Srivastava and S. Banerjee, *J. Nucl. Mater.* **224,** 146 (1995).
25. R. J. Borg, *J. appl. Phys.* **34,** 1562 (1973).